Design of all-normal dispersion microstructured optical fiber on silica platform for generation of pulse-preserving supercontinuum under excitation at 1550 nm

Igor A. Sukhoivanov, *Senior Member, IEEE*, Sergii O. Iakushev, Oleksiy V. Shulika, Enrique Silvestre, and Miguel V. Andrés

***Abstract*—We investigated numerically the possibility of all normal dispersion fiber design for near-infrared supercontinuum generation based on a standard air-silica microstructure. The design procedure includes finding of target dispersion profile and subsequent finding of appropriate geometrical fiber design by inverse dispersion engineering. It was shown that the tailoring of dispersion profile could increase the spectral width of generated supercontinuum while maintaining perfect spectral flatness. Conditions necessary for wide and flat supercontinuum generation as well as restrictions imposed by chosen materials were discussed. As a result of design and optimization procedure, an air-silica design was found providing normal dispersion up to 3 μm. Simulation results with 10 nJ, 100 fs pulses demonstrate supercontinuum generation up to 1.3 octave; whereas pumping with 30 nJ, 100 fs pulses could provide 1.8 octave supercontinuum.**

***Index Terms*— Supercontinuum generation; Microstructured fibers; Nonlinear optics, fibers; Ultrafast processes in fibers; Ultrafast nonlinear optics.**

I. Introduction

SUPERCONTINUUM (SC) generation is a very active field of research since 1970s [1]. Supercontinuum is the generation of intense ultrafast broadband radiation based on nonlinear interaction during propagation of ultrafast pulses focused into a transparent material. The supercontinuum can be generated in different states of matter liquids, solids and gases [1]. The spectra can cover the range from the ultraviolet to the near infrared and sometimes is called "white-light". This kind of radiation can be intense, collimated, and coherent similarly to conventional laser light. Owing to that supercontinuum has found numerous applications in optical communications, optical coherence tomography, frequency metrology, and extremely short pulse generation [1, 2]. The advent of microstructured optical fibers in the late 1990s has led to a significant progress in the generation of supercontinuum spectra [2]. The design freedom of microstructured fibers allowed supercontinuum generation in the wide range of pump sources. Particularly application of low energy nanojoule pump pulses allowed generation supercontinuum spectra covering more than one octave [2, 3]. The broadest SC spectra are generated usually when injecting the pump pulse into the anomalous group velocity dispersion (GVD) wavelength range of the fiber [3]. In this case the broadening mechanism is dominated by soliton dynamics and modulation instability [3, 4]. Pumping in anomalous dispersion region can lead to some problems such as complex temporal profile, the spectral fine structure, lack of spectral flatness, increment of noise, and low-coherence characteristics [5–7]. SC generation in normal dispersion region of the fiber also can provide octave spanning spectra [8, 9]. Over recent years were proposed all-normal dispersion photonic crystal fibers (ANDi PCFs) which exhibit normal dispersion profiles such that supercontinuum generation appears in the normal dispersion region of the fiber over the whole supercontinuum band [10]. The physical mechanism of SC generation in ANDi PCF is drastically different as compared to that one in anomalous region of the fibers. In normal dispersion region spectral broadening appears preliminary due to the action of self-phase modulation (SPM) and four-wave mixing (FWM) induced by optical wave breaking (OWB) [9, 11]. Pumping near the flattened top of such ANDi PCF provides generation of flat-top and octave-spanning SC characterized by a high degree of pulse-to-pulse coherence [12] and preserving a single pulse in temporal domain. Such flat and broad spectrum can enable constant signal-to-noise ratio (and constant dynamic range) in spectral measurements. Whereas maintaining of single pulse in temporal domain and smooth phase distribution are attractive for time-resolved measurements, amplification of SC pulses in parametric processes or

This paragraph of the first footnote will contain the date on which you submitted your paper for review. It will also contain support information, including sponsor and financial support acknowledgment. For example, "This work was supported in part by the U.S. Department of Commerce under Grant BS123456".

I. A. Sukhoivanov and O. V. Shulika are with Departamento de Ingeniería Electrónica y Comunicaciones, DICIS, Universidad de Guanajuato, Salamanca 36885, México (e-mail: oshulika@ugto.mx).

S. O. Iakushev is with Laser Development Department, Laser Zentrum Hannover e.V., Hollerithallee 8, D-30419 Hannover, Germany.

E. Silvestre is with Departamento de Óptica, Universidad de Valencia, Dr. Moliner 50, 46100 Burjassot, Spain.

M. V. Andrés is with Departamento de Física Aplicada y Electromagnetismo – ICMUV, Universidad de Valencia, Dr. Moliner 50, 46100 Burjassot, Spain.

for few-cycle pulse generation [9, 13].

ANDi fibers can be fabricated by standard stack-and-draw technique based on common air-silica microstructure. This way ANDi fibers having flattened top of dispersion curve for pumping at wavelengths 650 nm [9], 800 nm [14], 1060 nm [9, 15] were fabricated. However, providing of normal dispersion in the near infrared region (NIR) with air-silica PCFs is more difficult task and moreover their performance is limited also by increasing of absorption losses in silica in the near infrared. Therefore another materials and types of ANDi fibers were proposed for NIR SC generation. Particularly, germanium-doped silica ANDi fibers were proposed [16, 17]. For example, all-solid heavily Ge-doped fiber with a four-layer refractive index profile could provide flat normal dispersion up to 2600 nm allowing flat-top SC generation ranging from 1000 to 2600 nm [16]. However, high concentration of GeO_2 in the fiber core is required. Smaller concentration of GeO_2 can be used if additional air holes are inserted [17]. Hybrid fiber based on a silica cladding and yttria-alumino-silicate glass core was proposed providing high nonlinearity and a large refractive index difference with silica for dispersion engineering [18]. All-solid soft glass microstructured fibers also allow flexibility of dispersion engineering via manipulation of material dispersions of the pair of glasses [19-21]. Such soft glass fibers could provide normal dispersion up to 3500 nm [22]. Chalcogenide fibers are promising candidates for SC generation in the mid-infrared region due to their wide transmission range and large nonlinear refractive index [23-25]. For example, flat SC generation in chalcogenide fiber was reported in the region 3-5 μm [25].

An important point for designing of ANDi fibers is dispersion engineering. Dispersion profile can sufficiently influence the SC generation dynamics. Controlling of dispersion profile up to the higher dispersions order allows improve the width and flatness of the generated SC in ANDi fibers. This way was designed lead–silicate-based binary multi-clad microstructured fiber which could provide ultra wide (903–2443 nm) supercontinuum generation with perfect flatness (< 5 dB) [26]. Here we will show via numerical modeling that careful dispersion engineering in combination with powerful numerical optimization technique could enhance greatly the performance of conventional air-silica microstructured ANDi fibers. Variation of only geometrical fiber parameters (pith and air holes diameters) allows extend flat normal dispersion band up to 3 μm This allows SC generation up to 1.8 octaves with femtosecond nanojoule pulses. Limitations and perspectives of air-silica microstructured ANDi fibers as compared to other types of ANDi fibers are discussed.

II. Pulse Propagation in ANDi fiber

Ultrashort pulse propagation in optical fiber and particularly supercontinuum generation is simulated using generalized nonlinear Schrödinger equation (GNLSE). It is formulated in terms of the electric field envelope $A = A(z,T)$ at a propagation distance z in a retarded reference time frame $T = t - \beta_1 z$ traveling at the envelope group velocity β_1^{-1} [2, 11, 27]:

$$\frac{\partial A(z,T)}{\partial z} = -\frac{\alpha}{2}A(z,T) + \left(\sum_{k\geq 2}\frac{i^{k+1}}{k!}\beta_k\frac{\partial^k}{\partial T^k}\right)A(z,T) + i\gamma\left(1+\frac{i}{\omega_0}\frac{\partial}{\partial T}\right)\times\left(A(z,T)\int_{-\infty}^{\infty}R(\tau)\left|A(z,T-\tau)\right|^2 d\tau\right), \quad (1)$$

where α is the attenuation constant, γ is the nonlinear coefficient, β_n are the dispersion coefficients obtained by a Taylor series expansion of the propagation constant $\beta(\omega)$ around the pulse center frequency ω_0. The pulse center frequency corresponds to the wavelength of 1550 nm in our study. The response function $R(t) = (1-f_R)\delta(t) + f_R h_R(t)$ includes both the instantaneous electronic and delayed Raman contributions, with $f_R = 0.18$ representing the fractional contribution of the delayed Raman response. For the Raman response function of the silica fiber, $h_R(t)$, the analytical expression is used [28]:

$$h_R(t) = \frac{\tau_1^2+\tau_2^2}{\tau_1\tau_2}\exp\left(-\frac{t}{\tau_2}\right)\sin\left(\frac{t}{\tau_1}\right), \quad (2)$$

where $\tau_1 = 12.2$ fs and $\tau_2 = 32$ fs.

The GNLSE (1) is solved by Runge–Kutta in the interaction picture method [2].

III. Starting Characteristics

Previous results related to the designing of ANDi fibers have shown that pumping near the top of convex dispersion curve is optimal for supercontinuum generation in ANDi fibers [9, 11]. Therefore, we have chosen for the starting design the convex dispersion profile having top near 1550 nm shown in the Fig. 1(a). This dispersion profile is described by the following set of dispersion coefficients: $\beta_2 = 1.6735\times10^{1}\left(\text{ps}^2/\text{km}\right)$, $\beta_3 = -3.790\times10^{-2}\left(\text{ps}^3/\text{km}\right)$, $\beta_4 = 2.6110\times10^{-4}\left(\text{ps}^4/\text{km}\right)$, $\beta_5 = -8.0617\times10^{-7}\left(\text{ps}^5/\text{km}\right)$, $\beta_6 = 2.1365\times10^{-9}\left(\text{ps}^6/\text{km}\right)$, $\beta_7 = -3.6457\times10^{-12}\left(\text{ps}^7/\text{km}\right)$, $\beta_8 = -1.0578\times10^{-14}\left(\text{ps}^8/\text{km}\right)$, $\beta_9 = 1.35\times10^{-16}\left(\text{ps}^9/\text{km}\right)$. This dispersion curve was inspired by the dispersion profile of air-silica ANDi PCF which we have developed earlier for 800 nm [14]. We use it as a starting dispersion profile for subsequent dispersion engineering.

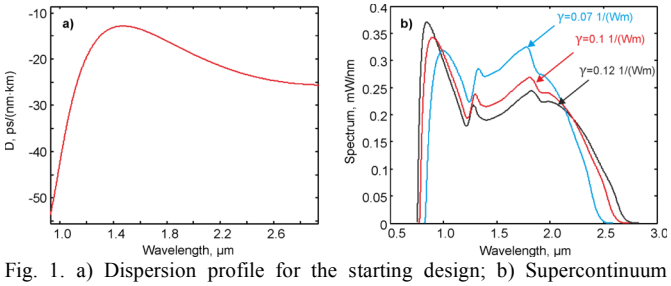

Fig. 1. a) Dispersion profile for the starting design; b) Supercontinuum spectra obtained in the case of dispersion profile shown in (a) and for various values of the nonlinear coefficient.

Figure 1(b) shows supercontinuum spectra obtained for starting dispersion profile at 1550 nm for different amounts of nonlinear coefficient. Pump pulse energy was chosen to be $E_0 = 5\,\text{nJ}$, pulse duration FWHM = 100 fs, pulse shape – Gaussian, fiber length 10 cm. From Fig.1 we can see that such dispersion profile could provide wide supercontinuum generation at 1550 nm. For $\gamma = 0.07$ 1/(W·m) spectral width (SW) is 1.59 octave (at the level −20 dB), whereas the drop of spectral intensity in the central part of the spectrum (DP) is only −1.6 dB. So, we can obtain wide spectrum with good flatness.

Increasing of nonlinear coefficient provides wider spectrum but the dip in the central part becomes stronger, such that pulse energy transfers form the central part (pumping wavelength) to the lateral bands of the spectrum. Owing to that for $\gamma = 0.1$ 1/(Wm)we have SW = 1.77, DP = −2.5 dB; whereas for $\gamma = 0.12$ 1/(Wm) we have SW = 1.86, DP = −3.2 dB. In the last case the dip is already larger than 3 dB, in order to maintain the perfect flatness we are trying here to maintain it no more than 3 dB. The depletion of the central part of the spectrum and appearance of the dip actually limits the performance of the given fiber, because we cannot increase further the spectral width without worsening the spectral flatness [14]. However, the significant advantage of microstrcuctured optical fibers is the possibility to tailor the dispersion profile in the wide range, which can increase the performance of the fiber for a given application. At the next step we investigate the possibility to tailor starting dispersion profile in order to increase the spectral width while maintaining good spectral flatness.

A. Variation of Dispersion Profile

For the next step we have chosen dispersion profile shown in the Fig. 1 a) and nonlinear coefficient $\gamma = 0.12$ 1/(W·m) providing wider bandwidth but excessive spectral dip DP = −3.2 dB as Fig. 1 b) shows. The aim of dispersion engineering is to tune dispersion profile in order to improve the spectral flatness (maintain the dip at the level ≤ -3 dB) and expand spectral width of the generated SC. We tune dispersion coefficients, shown in Sec. 3 "STARTING DESIGN", separately, starting from $\beta_2 = 1.6735\times10^{1}\left(\text{ps}^2/\text{km}\right)$.

Figure 2(a) shows supercontinuum spectra obtained by tuning β_2. Pump pulse parameters are the same for all cases (pulse energy – 5 nJ, pulse duration – 100 fs, pulse shape – Gaussian, fiber length 10 cm). If changes in the pump parameters are made, it will be noted in the text below. From

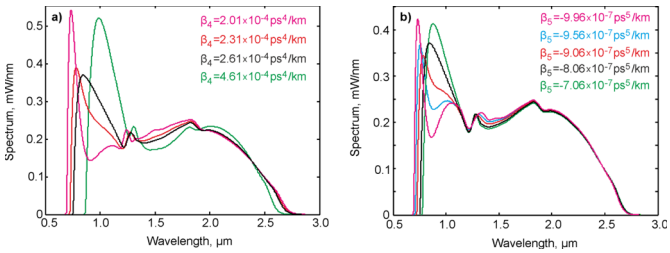

Fig. 3. a) Supercontinuum spectra obtained by tuning β_4; b) supercontinuum spectra obtained by tuning β_5

Fig.2(a) we can see that if we take larger $\beta_2 = 2.67\times10^{1}\left(\text{ps}^2/\text{km}\right)$ one can reduce the red spectral peak in the longer wavelength side of the spectrum, but the spectral width also is reduced comparing to the initial value of β_2. Whereas smaller β_2 leads to the increasing of the red spectral peak. So, tuning of β_2 does not lead to the improvement of spectral profile namely improvement of the flatness and extending of the spectrum. The same conclusion one can make for tuning of β_3 shown in the Fig. 2(b). In this case any changes of β_3 does not lead to the reduction of the red spectral peak.

Figure 3 shows supercontinuum spectra obtained by tuning β_4 and β_5. Tuning of β_4 also does not lead to the improvement of spectrum as Fig. 3(a) shows. However, from Fig. 3(b) one can see that there is some range when red spectral peak is reduced whereas spectral width becomes larger when we tune β_5.

Figure 4 a) shows the enlarged at the shorter wavelength side figure of the β_5 tuning. Form this figure one can clearly see that smaller $\beta_5 = -9.06\times10^{-7}\left(\text{ps}^5/\text{km}\right)$ indeed reduces red spectral peak of the spectrum (DP = −2.8 dB) and provides larger spectral width (SW = 1.91 octave) as compared to the initial value of $\beta_5 = -8.06\times10^{-7}\left(\text{ps}^5/\text{km}\right)$. Further decreasing of β_5 up to $\beta_5 = -9.56\times10^{-7}\left(\text{ps}^5/\text{km}\right)$ leads again to wider spectrum (SW=1.94 octave), the drop of spectral intensity is DP = −3 dB. Finally for $\beta_5 = -9.96\times10^{-7}\left(\text{ps}^5/\text{km}\right)$, we have SW=1.97 octave and DP = −4 dB. So we see that $\beta_5 = -9.56\times10^{-7}\left(\text{ps}^5/\text{km}\right)$ is optimal because spectral width becomes larger (SW = 1.94 octave) while spectral flatness is still at optimal level (DP = −3 dB).

Figure 4 b) shows dispersion profiles corresponding to the tuning of β_5. Dispersion curves nearly coincides in the wavelength range larger 1.5 μm, therefore it is shown only the shorter wavelength part for better viewing. From this figure one can see that the difference between dispersion curves appears only for $\lambda < 1.1\,\mu\text{m}$. It is obvious that this provides the changes in the shorter wavelength side of supercontinuum spectra shown in the Fig. 4(a). Particularly the value $\beta_5 = -9.56\times10^{-7}\,(\text{ps}^5/\text{km})$ corresponds to the more flattened top of dispersion curve as compared to the initial value $\beta_5 = -8.06\times10^{-7}\,(\text{ps}^5/\text{km})$. In other words, the flattened top of dispersion curve is more extended to shorter wavelengths such that the drop of dispersion curve is blue-shifted. We assume that this wider flattened top towards shorter wavelength side provides more flat and at the same time wider spectrum as Fig. 4 a) shows. However, further reduction of β_5 up to the $\beta_5 = -9.96\times10^{-7}\,(\text{ps}^5/\text{km})$, provides again wider spectrum SW=1.97, but spectral flatness becomes worth DP = −4 dB. We assume that this is related to the stronger gradient of dispersion curve at the edge in this case, i.e. flattened top of dispersion curve becomes even larger, but the drop of dispersion curve at the edge becomes faster. Owing to that $\beta_5 = -9.56\times10^{-7}\,(\text{ps}^5/\text{km})$ is optimal compromise in this case. We have investigated tuning of dispersion coefficients also for β_6, and β_7; however it has not provided further sufficient increasing of spectral width while maintaining good flatness.

Thus, we can choose dispersion coefficients from Sec.3 "STARTING DESIGN" together with new $\beta_5 = -9.56\times10^{-7}\,(\text{ps}^5/\text{km})$ and $\gamma = 0.12\ \ 1/(\text{W}\cdot\text{m})$ as a target design for the next step. It allows to increase spectral width up to nearly two octaves (SW = 1.94 octave), while maintaining excellent spectral flatness (DP = −3 dB). Fig.5(a) shows corresponding spectrum.

Thus, dispersion engineering could provide indeed increasing of the spectral width of SC generated in ANDi fibers while maintaining perfect spectral flatness, however the limiting factor in this case can be the drop of dispersion curve from the short wavelength side due to the material dispersion leading to the increasing of spectral oscillations at the short wavelength side of the spectrum. The possible difficulty can be also a large amount of nonlinear coefficient $\gamma = 0.12\ \ 1/(\text{W}\cdot\text{m})$ which would be difficult to realize at 1550 nm in air-silica fiber as compared to e.g. 800 nm. We have estimated the influence of smaller nonlinear coefficient on the SC generation. Fig. 5 b) shows spectra for different amounts of nonlinear coefficient. Particularly if we reduce nonlinear coefficient up to $\gamma = 0.06\ \ 1/(\text{W}\cdot\text{m})$ the spectral width of the SC sufficiently reduces up to SW = 1.6 octave (DP = −1.7 dB). However, the possible solution is increasing of pump pulse energy from 5 nJ till 10 nJ. In this case we can maintain the wide spectrum (SW = 1.94 octave) and spectral flatness at the same level (DP = −3 dB), when nonlinear coefficient is smaller.

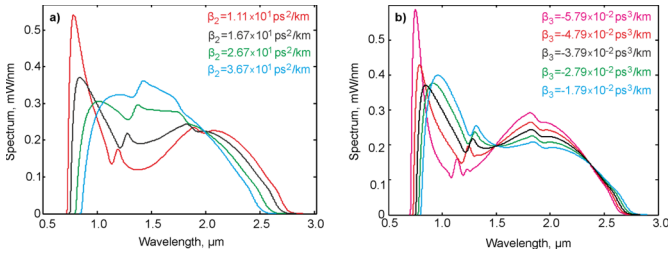

Fig. 2. a) Supercontinuum spectra obtained by tuning β_2; b) supercontinuum spectra obtained by tuning β_3

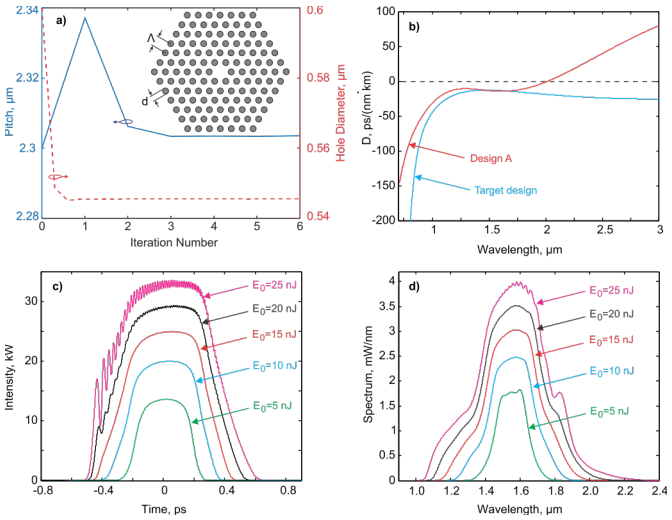

Fig. 6. Supercontinuum generation for the **design A**. a) air-silica microstructure having fused silica solid core and hexagonal lattice of equal air holes, pitch $\Lambda = 2.304\,\mu\text{m}$, diameter of holes $d = 0.546\,\mu\text{m}$, core diameter is 4.054 μm; b) dispersion profiles for the target design and design A; c) pulse intensity profiles after propagation in 10 cm length fiber; c) spectral intensity profiles after propagation in 10 cm length fiber.

IV. TRANSFORMING DISPERSION CURVE INTO PCF TOPOLOGY

The next step is finding of specific air-silica microstructures which could provide dispersive characteristics and nonlinear coefficient close to the target values found in previous section. Calculation of modal and dispersive properties of air-silica microstructures have been made using a Fourier based modal technique [29] and optimization has been made by a gradient-based algorithm [30]. The merit function was the root mean square of the difference between the target dispersion and the dispersion of a given design in a certain wavelength range.

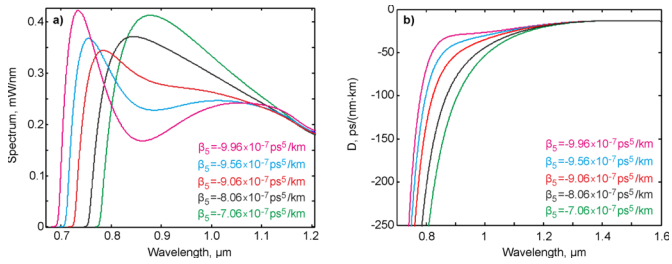

Fig. 4. a) Supercontinuum spectra obtained by tuning β_5 (enlarged Fig. 3(b) at the shorter wavelength side); b) Dispersion profiles corresponding to the tuning of β_5

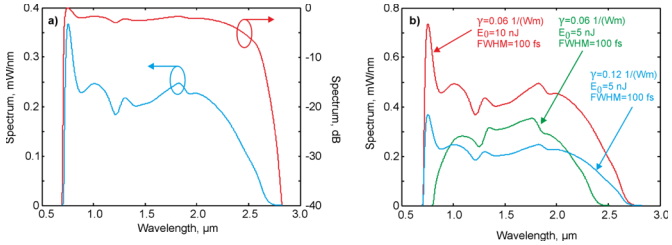

Fig. 5. a) Supercontinuum spectrum in linear and logarithmic scale obtained for target design; b) Influence of nonlinear coefficient and pump energy variation on SC generation for the target design.

Once the target dispersion $D(\lambda)$ is fixed, a finite number N_λ of sampling wavelengths λ_k, $(k=1,2,\quad,N_\lambda)$ is chosen within a given working wavelength range $\left[\lambda_1,\lambda_{N_\lambda}\right]$. Thus, the merit function is evaluated by means of the expression:

$$\chi^2(p)=\frac{1}{N_\lambda}\sum_{k=1}^{N_\lambda}\left\{D(p,\lambda_k)-D^{\text{target}}(\lambda_k)\right\}^2, \qquad (3)$$

where $p=(p_1,p_2,p_3,\quad)$ is the set of parameters defining the PCF. In the basic case $p=(\Lambda,d)$, where Λ is the pitch and d the diameter of holes (see Fig. 6), while in a more complex case we will consider a PCF with two different hole sizes and consequently $p=(\Lambda,d_1,d_2)$ (see Fig. 7 and 8).

Given a point in the parameter space $p_{(m)}$, we evaluate $\beta(\lambda_k)$, using the Fourier based modal technique, then $\beta_1(\lambda_k)$ is evaluated analytically using the Hellmann–Feynman theorem as it is described in Ref. [29]. Finally we evaluate $\beta_2(\lambda_k)$ – and $D(\lambda_k)$ – calculating numerically the derivative of $\beta_1(\lambda_k)$. To reach the minimum of the merit function, we evaluate the derivatives of D with respect to the parameters, $\partial_p D\left(p_{(m)},\lambda_k\right)$. First, using again the Hellmann–Feynman theorem we compute $\partial_p\beta\left(p_{(m)},\lambda_k\right)$ as it is describer with detail in Ref. [30] and then numerically the derivatives of β_1 and β_2. Thus, we obtain a linear approximation for $D\left(p_{(m)},\lambda_k\right)$:

$$D^{lin}(p,\lambda_k)=D\left(p_{(m)},\lambda_k\right)+\partial_p D\left(p_{(m)},\lambda_k\right)\cdot\left(p-p_{(m)}\right), \qquad (3)$$

which provides a quadratic local approximation of the merit function, minimum of which determines the new set of parameters $p_{(m+1)}$. This new point in the parameter space gives a dispersion closer to the target and is used as the starting point for a new iteration. Typically, convergence is achieved with less than 20 iterations.

In our calculations we have used the Sellmeier coefficients reported by J. W. Fleming in [33], where the wavelength range 0.3650–4.2809 μm was used. Thus, we assume that such values can be used up to 3 μm, although we are aware that the material absorption will limit the usefulness of our results above 2.4 μm.

We have found three air-silica microstructures referred here to as **designs A**, **B1**, and **B2**, which are providing dispersion profiles close to the target one.

A. Design A

At first, we investigated simple microstructures having fused silica solid core and hexagonal lattice of equal air holes, shown in the inset of Fig. 6(a). In this case, the optimization of the merit function was carried out in the wavelength range [800, 1800] nm. In this case, the starting point in the parameter space was Λ = 2.3 μm and d = 0.6 μm and the convergence was achieved with 5 iterations. The Fig. 6(a) shows the evolution of the parameters along the iterative process. Dispersion profiles for the target design and the actually obtained fiber design are shown in the Fig. 6(b). Form this figure we can see that dispersion curves perfectly coincides around the pump wavelength 1550. The amount of normal dispersion at wavelength 1550 nm is $D = -14.1$ ps/(nm·km). Design A demonstrates dispersion peak shifted to the shorter wavelength as compared to the target design. This is rather advantage, because one can expect expanding of the spectra stronger to the shorter wavelength side. However, there are some drawbacks in this design. Particularly there is a quite narrow bandwidth of flat-top normal dispersion around 1550 nm and moreover for $\lambda > 2\,\mu$m dispersion becomes anomalous. Nonlinear coefficient is very small $\gamma = 0.003$ 1/(W·m) at 1550 nm.

The results of supercontinuum generation depending on the pump energy are shown in the Fig. 6(c) and Fig. 6 d). For the energies 5-10 nJ spectral broadening is insufficient. Spectral shapes are similar to SPM broadened spectra [9, 27], but we do not see the development of lateral bands due to the action of OWB and FWM typical for SC generation in ANDi fibers [9]. This can be attributed to the small nonlinear coefficient and limited narrow bandwidth of flat-top normal dispersion around 1550 nm. Steep dispersion profile prevents effective spectral broadening due to the FWM. Owing to that the spectral width is smaller (SW=0.62 octave for 10 nJ pump energy) as compared to the target design.

We can increase further spectral width by increasing the pump power, but starting from 20 nJ spectrum extends beyond $\lambda = 2\,\mu$m such that spectral broadening appears partly in the anomalous dispersion region of the fiber. Owing to that we can see the degradation of the temporal pulse shape as Fig. 6(c) shows. So, we can conclude that the design A is not so good. The limited normal dispersion band is a strong limiting factor, it does not allow obtain wide spectrum and maintain good temporal pulse profile, which is a key advantage of SC generation in ANDi fibers.

B. Design B1

Next we investigate more complex air-silica microstructure having fused silica solid core and hexagonal lattice of air holes where the diameters of holes in the first inner ring and the outer rings are different. The optimization algorithm was applied in the wavelength range [800, 2800] nm and design B1 was obtained, as the inset of Fig. 7(b) shows, in which the air holes of the inner ring need to have a diameter smaller than the rest of the holes. The starting point in the parameter space was Λ = 2.3 μm and d_1 = d_2 = 0.54 μm and converge was achieved after 20 iterations. The Fig. 7(a) shows the evolution of the parameters along the iterative process. In this case, dispersion is normal at least up to $3\,\mu m$ as Fig. 7(b) shows. Design B1 also demonstrates flattened top of dispersion profile extended to the shorter wavelength as compared to the target design. However, one has to note that top of dispersion curve is shifted to $1.1\,\mu m$. The amount of normal dispersion at wavelength 1550 nm is larger here $D = -17.4\,ps/(nm \cdot km)$. Nonlinear coefficient $\gamma = 0.017\ \ 1/(W \cdot m)$ is also smaller as compared to the target design, but it is larger as compared to design A. The results of supercontinuum generation depending on the pump energy are shown in the Fig. 7(c) and Fig. 7(d). For the energies 5-10 nJ spectral broadening is also insufficient here due to the low nonlinear coefficient. Owing to that the spectral width is smaller (SW=1.32 octave for 10 nJ pump energy) as compared to the target design. However, the difference here is that we can increase pump power, due to the wider normal dispersion bandwidth. For example, for $E_0 = 30\,nJ$ we have SW=1.99 octave and DP = −3 dB; for $E_0 = 40\,nJ$ we have SW=2.18 octave and DP = −3 dB. So, we can see that the design B1 is quite attractive. One can obtain here spectral width larger 2 octaves, it is even larger as compared to the target design. However, we have to use quite large initial pulse energy 30-40 nJ in order to exploit properly the whole normal dispersion bandwidth. Increasing of nonlinear coefficient would allow reducing the necessary pump pulse energy. But even for 10 nJ initial pump energy we can obtain octave spanning spectral width (SW = 1.32 octave).

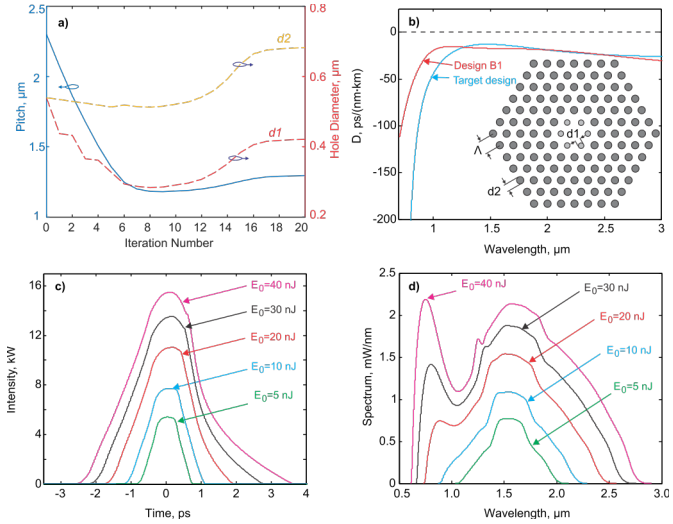

Fig. 7. Supercontinuum generation for the **design B1**. a) air-silica microstructure having fused silica solid core and hexagonal lattice of air holes, pitch $\Lambda = 1.295$ μm, diameters of air holes in the first inner ring are $d1 = 0.422$ μm, diameters of air holes in the outer rings are $d2 = 0.682$ μm, core diameter is 2.168 μm; b) dispersion profiles for the target design and design B1; c) pulse intensity profiles after propagation in 10 cm length fiber; c) spectral intensity profiles after propagation in 10 cm length fiber.

C. *Design B2*

Finally, we investigate the same air-silica microstructure as in design B1, but with different amount of inner and outer holes (design B2) a second fiber design was obtained by choosing a different wavelength range for the optimization algorithm. In this case, the wavelength in which the merit function was minimized was [700, 2800] nm and design B2 was obtained, shown in the inset of Fig. 8(b). Here, the starting parameters were as in case B1 and convergence was also achieved after 20 iterations. The design B2 has both inner and outer holes diameters smaller than the values of design B1, which makes the fabrication of this fiber B2 more challenging than previous fiber B1. In this case, dispersion is also normal up to $3\,\mu m$ as Fig. 8(b) shows. Design B2 demonstrates also flattened top of dispersion profile extended to the shorter wavelength as compared to the target design. The top of dispersion curve here is located exactly at the pump wavelength 1550 nm, however it is closer to the zero, i.e. the amount of normal dispersion at the pump wavelength is smaller in this case ($D = -6.9\,ps/(nm \cdot km)$). Nonlinear coefficient is $\gamma = 0.013\ \ 1/(W \cdot m)$. The results of supercontinuum generation depending on the pump energy are shown in the Fig. 8(c) and Fig. 8 d). In this case we can see fast development of lateral spectral bands due to FWM. However generation of novel shorter and longer wavelength spectral components is inefficient. Energy transferred from the central part of the spectrum is concentrated in the spectral peaks around 1050 nm and 1800 nm. Such that already at $E_0 = 10\,nJ$ the dip arise at 1550 nm (DP = −3.2 dB), whereas spectral width here (SW = 1.20) is smaller as compared to the Design B1 (SW = 1.32) for the same pump pulse energy. If we increase pump energy up to

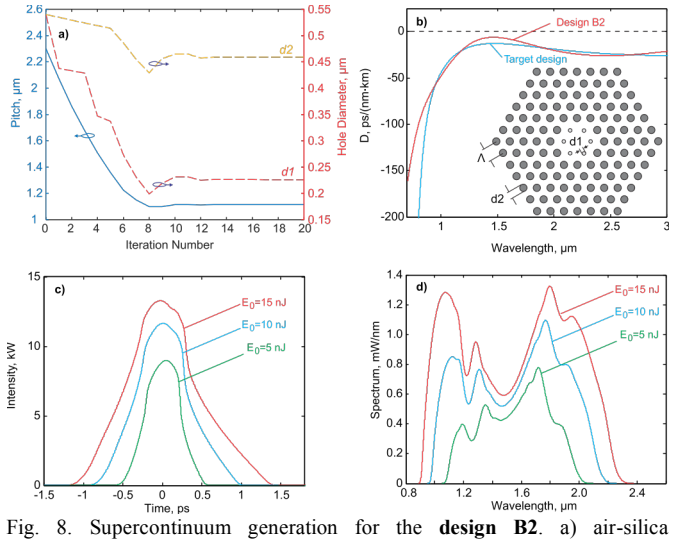

Fig. 8. Supercontinuum generation for the **design B2**. a) air-silica microstructure having fused silica solid core and hexagonal lattice of air holes, pitch $\Lambda = 1.113$ μm, diameters of air holes in the first inner ring are $d1 = 0.226$ μm, diameters of air holes in the outer rings are $d2 = 0.458$ μm, core diameter is 2.0 μm; b) dispersion profiles for the target design and design B2; c) pulse intensity profiles after propagation in 10 cm length fiber; c) spectral intensity profiles after propagation in 10 cm length fiber.

$E_0 = 15\,\text{nJ}$, we obtain SW = 1.35 octave and DP = −3.5 dB. The fast development of the spectral dip already at 10 nJ can be related to smaller amount of normal dispersion at 1550 nm in design B2 as compared to the design B1. Smaller amount of normal dispersion leads to the enhanced relative action of nonlinear effects [27] and potentially should increase spectral broadening. However, the impact of dispersion slope also becomes more important when dispersion peak is close to zero. In the Design B2 dispersion slope is enough to restrict gradual generation of novel wavelength spectral component shorter 1000 nm and longer 2200 nm.

Thus, we can conclude that the design B2 has clear drawbacks. Dynamics of SC generation is fast and the strong spectral dip in the central part arises already at quite low pump energy. This leads to the worsening of the spectral flatness while the spectral width is not so wide as compared to Design B1.

V. Discussion

Results presented in previous section shows that the design B1 is the most attractive. It allows obtaining supercontinuum larger than 2 octaves with good spectral flatness (DP = −3 dB).

From the presented analysis we can summarize also some other details important for designing and optimization of ANDi PCF. One has to maintain normal dispersion in the whole spectral band occupied by SC for maintaining stable pulse in temporal domain. Extending of the flattened top of dispersion profile to the shorter wavelength allows wider SC generation at shorter wavelength side of the spectrum. The amount of normal dispersion at the pump wavelength has to be quite large ($D \sim -14\ \text{ps/(nm}\cdot\text{km)}$). But we have to note also some limitations of the presented analysis. The GNLSE (1) does not include spectral dependence of nonlinear coefficient. However, its influence on SC generation in ANDi fibers has been already investigated [9, 19, 20]. Spectral variation of nonlinear coefficient theoretically would lead to the stronger broadening in the shorter wavelength side of the spectrum and smaller broadening in the longer wavelength side of the spectrum. However, comparison with experiment does not prove this estimation [9, 19, 20]. Moreover constant nonlinear coefficient in (1) provides better matching with experiment [9]. Probably this can be related to the specific spectral broadening mechanism in ANDi fiber [9].

An important limiting factor is material loss in silica which increases strongly for $\lambda > 2.4\,\mu\text{m}$ [31], this can limit the supercontinuum width at longer wavelength side in air-silica microstructure. For example, if we take design B1 for $E_0 = 30\,\text{nJ}$ we have SW = 1.99 octave as Fig. 7 d) shows. Cutting of spectral intensity at $2.4\,\mu\text{m}$ gives SW = 1.84.

Another important issue is that the nonlinear coefficient in the Design B1 is smaller as compared to the target design. Therefore, it is necessary to use quite large initial pulse energy 30-40 nJ in order to exploit the whole normal dispersion bandwidth. Modern commercial compact femtosecond fiber lasers could deliver already up to 50 nJ pulse energy at 1550 nm [32]. However, application of lower energy pulses would be more beneficial. Increasing of nonlinear coefficient would allow reducing the necessary pump pulse energy. This can be done without the changing of materials in the fiber by modification of only geometrical structure to provide smaller effective mode area. However the changes of effective mode area via the variation of geometrical structure will influence the dispersion profile as well. But in this particular case one can see that designs B1 and B2 provides excessive band of normal dispersion (ZDW point located at wavelength longer 3 μm), which cannot be fully exploited in air-silica fibers due to the increased absorption in silica at the wavelengths longer 2.4 μm. Therefore it is natural to impose constrain on the width of normal dispersion band up to 2.4 μm in the optimization algorithm. This should give more freedom to the numerical algorithm when searching the minimum of merit function. In other words one can increase nonlinear coefficient via the price of worsening of dispersion profile at wavelengths larger 2.4 μm. But in order to ensure the finding of minima with smaller effective mode area one has to modify directly the merit function by including evaluation of effective mode area relative to some target effective mode area. The relative contributions of effective mode area and dispersion into the merit function can be tuned by weight coefficients. We are going to include the mentioned possibility into our numerical algorithm.

Results obtained after numerical optimization clearly show that the potential of air-silica ANDi PCFs is still not fully exploited. Up to now the designing of such fibers were limited by variation of the pitch and diameter of equal air holes in the hexagonal lattice [9, 11, 14, 15]. But additional flexibility can be achieved via e.g. variation of air holes diameters in each ring. One can see that the changing of air holes diameter in only one inner ring (Designs B1, B2) can significantly expand normal dispersion band up to 3 μm. This can support potentially huge SC generation up to two octaves and more. However, the expanding of SC towards longer wavelengths is limited by absorption in silica. Therefore, for the wavelength region > 2.4 μm e.g. soft glasses or chalcogenide fibers have to be used. On the other side SC in air-silica ANDi PCFs can be expanded to shorter wavelengths. This can be done by extending the flat top of dispersion curve towards shorter wavelengths. It was shown that the top of dispersion curve can be shifted at least up to 600 nm such that visible SC generation is possible [9]. However, the dispersion slope was quite strong in the fiber proposed in [9] preventing SC generation towards near infrared. We believe that proper dispersion engineering and numerical optimization would provide finding of novel air-silica ANDi PCFs designs allowing SC generation up to two octaves covering visible and NIR regions.

VI. Conclusion

In order to optimize the fiber supercontinuum generation in all-normal dispersion regime at 1550 nm, it has been found particularly useful to split the procedure in to steps. First we investigated the optimum dispersion profile that leads to the broadest and flattest supercontinuum spectrum. Second, several air-silica microstructured fibers have been proposed, which provide the best fit to the target dispersion profile within a certain wavelength range, assuming either an uniform microstructure or air holes or a microstructure with two different sizes of air holes. Our results show that it is feasible to fab-

ricate an air-silica microstructured fiber with normal dispersion up to $3\,\mu m$ and nonlinear coefficient $\gamma = 0.017\ 1/(W \cdot m)$ at 1550 nm. Although the nonlinear coefficient is relatively small with respect the values that are achievable in all-normal fibers at 800−1100 nm, we have demonstrated that pumping with 10 nJ and 100 fs pulses provides supercontinuum generation of 1.3 octave; whereas increasing the pump up to 30 nJ would generate a 1.8 octave supercontinuum.

REFERENCES

[1] R. R. Alfano (Ed.), *The Supercontinuum Laser Source*, 2nd ed. (Springer, 2006).

[2] J. M. Dudley, J. R. Taylor (Eds.), *Supercontinuum Generation in Optical Fibers* (Cambridge 2010).

[3] J. M. Dudley, G. Genty, and S. Coen, "Supercontinuum generation in photonic crystal fiber," Rev. Mod. Phys. **78**, 1135–1184 (2006).

[4] J. Herrmann, U. Griebner, N. Zhavoronkov, A. Husakou, D. Nickel, J. Knight, W. Wadsworth, P. S. J. Russell, and G. Korn, "Experimental evidence for supercontinuum generation by fission of higher-order solitons in photonic crystal fibers," Phys. Rev. Lett. **88**, 173901 (2002).

[5] X. Gu, L. Xu, M. Kimmel, E. Zeek, P. O'Shea, A. P. Shreenath, R. Trebino, and R. S. Windeler, "Frequency-resolved optical gating and single-shot spectral measurements reveal fine structure in microstructure-fiber continuum," Opt. Lett. **27**, 1174–1176 (2002).

[6] K. L. Corwin, N. R. Newbury, J. M. Dudley, S. Coen, S. A. Diddams, K. Weber, and R. S. Windeler, "Fundamental noise limitations to supercontinuum generation in microstructure fiber," Phys. Rev. Lett. **90**, 113904 (2003).

[7] N. R. Newbury, B. R. Washburn, and K. L. Corwin, "Noise amplification during supercontinuum generation in microstructure fiber," Opt. Lett. **28**, 944–946 (2003).

[8] N. Nishizawa and J. Takayanagi, "Octave spanning high-quality supercontinuum generation in all-fiber system," J. Opt. Soc. Am. B **24**, 1786–1792 (2007).

[9] A. M. Heidt, A. Hartung, G. W. Bosman, P. Krok, E. G. Rohwer, H. Schwoerer, and H. Bartelt, "Coherent octave spanning near-infrared and visible supercontinuum generation in all-normal dispersion photonic crystal fibers," Opt. Express **19**(4), 3775–3787 (2011).

[10] A. Hartung, A. M. Heidt, and H. Bartelt, "Design of all-normal dispersion microstructured optical fibers for pulse-preserving supercontinuum generation," Opt. Express **19**, 7742-7749 (2011).

[11] A. M. Heidt, "Pulse preserving flat-top supercontinuum generation in all-normal dispersion photonic crystal fibers," J. Opt. Soc. Am. B **27**(3), 550–559 (2010).

[12] M. Klimczak, G. Soboń, R. Kasztelanic, K. M. Abramski & R. Buczyński, Direct comparison of shot-to-shot noise performance of all normal dispersion and anomalous dispersion supercontinuum pumped with sub-picosecond pulse fiber-based laser, Scientific Reports **6**, 19284, (2016).

[13] A. M. Heidt, J. Rothhardt, A. Hartung, H. Bartelt, E. G. Rohwer, J. Limpert, and A. Tünnermann, "High quality sub-two cycle pulses from compression of supercontinuum generated in all-normal dispersion photonic crystal fiber," Opt. Express **19**, 13873-13879 (2011).

[14] I. A. Sukhoivanov, S. O. Iakushev, O. V. Shulika, J. A. Andrade-Lucio, A. Díez, and M. Andrés, "Supercontinuum generation at 800 nm in all-normal dispersion photonic crystal fiber," Opt. Express 22, 30234-30250 (2014).

[15] L. E. Hooper, P. J. Mosley, A. C. Muir, W. J. Wadsworth, and J. C. Knight, "Coherent supercontinuum generation in photonic crystal fiber with all-normal group velocity dispersion," Opt. Express 19(6), 4902–4907 (2011).

[16] C. C. Wang, M. H. Wang, and J. Wu, "Heavily Germanium-Doped Silica Fiber With a Flat Normal Dispersion Profile", IEEE Photonics Journal 7, 7101110, 2015.

[17] K. Tarnowski and W. Urbanczyk, "All-Normal Dispersion Hole-Assisted Silica Fibers for Generation of Supercontinuum Reaching Midinfrared", IEEE Photonics Journal 8, 7100311, 2016.

[18] X. Li, J. Li, T. Cheng, D. Chen, S. Zheng, W. Bi, W. Gao, Y. Ohishi, L. Hu, and M. Liao, "Silicate glass hybrid fiber with all-normal dispersion for coherent supercontinuum", Journal of Lightwave Technology PP, 1, 2016.

[19] G Stepniewski, M Klimczak, H Bookey, B Siwicki, D Pysz, R Stepien, A K Kar, A J Waddie, M R Taghizadeh and R Buczynski, "Broadband supercontinuum generation in normal dispersion all-solid photonic crystal fiber pumped near 1300 nm", Laser Phys. Lett. 11, 055103, (2014).

[20] M. Klimczak, B. Siwicki, P. Skibiński, D. Pysz, R. Stępień, A. Heidt, C. Radzewicz, and R.Buczyński, "Coherent supercontinuum generation up to 2.3 μm in all-solid soft-glass photonic crystal fibers with flat all-normal dispersion," Opt. Express 22, 18824-18832 (2014).

[21] T. Martynkien, D. Pysz, R. Stępień, and R. Buczyński, All-solid microstructured fiber with flat normal chromatic dispersion, Optics Letters 39, 2342-2345, (2014).

[22] B. Siwicki, R. Kasztelanic, M. Klimczak, J. Cimek, D. Pysz, R. Stępień and R. Buczyński, "Extending of flat normal dispersion profile in all-solid soft glass nonlinear photonic crystal fibers", Journal of Optics 18, 065102, 2016.

[23] P. S. Maji and P. R. Chaudhuri, Design of all-normal dispersion based on multimaterial photonic crystal fiber in IR region for broadband supercontinuum generation, Applied Optics 54, 4042-4048, 2015.

[24] L. Liu, T. Cheng, K. Nagasaka, H.Tong, G. Qin, T. Suzuki, and Y. Ohishi, "Coherent mid-infrared supercontinuum generation in all-solid chalcogenide microstructured fibers with all-normal dispersion", Optics Letters 41, 392-395, 2016.

[25] S. Kedenburg, T. Steinle, F. Mörz, A. Steinmann, and H. Giessen, High-power mid-infrared high repetition-rate supercontinuum source based on a chalcogenide step-index fiber, Optics Letters 40, 2668-2671, 2015.

[26] S. K. Chatterjee, S. N. Khan, and P. R. Chaudhuri, "Designing a two-octave spanning flat-top supercontinuum source by control of nonlinear dynamics through multi-order dispersion engineering in binary multi-clad microstructured fiber", Journal of the Optical Society of America B 32, 1499-1509, 2015.

[27] G. P. Agrawal, *Nonlinear Fiber Optics*, 4th ed. (Academic Press, Boston, 2007).

[28] K. J. Blow and D. Wood, "Theoretical Description of Transient Stimulated Scattering in Optical Fibers", IEEE J. Quantum Electron. **25**, 2665-2673 (1989).

[29] E. Silvestre, T. Pinheiro-Ortega, P. Andrés, J. J. Miret, and A. Ortigosa-Blanch, "Analytical evaluation of chromatic dispersion in photonic crystal fibers," Opt. Lett. **30**, 453–455 (2005).

[30] D. Castelló-Lurbe, V. Torres-Company, and E. Silvestre, "Inverse dispersion engineering in silicon waveguides," J. Opt. Soc. Am. B **31**, 1829-1835 (2014).

[31] O. Humbach, H. Fabian, U. Grzesik, U. Haken, W. Heitmann, "Analysis of OH absorption bands in synthetic silica", Journal of Non-Crystalline Solids **203**, 19-26 (1996).

[32] E.g. Carmel X-series from Calmarlaser: www.calmarlaser.com.

[33] J. W. Fleming, "Dispersion in GeO_2-SiO_2 glasses," Applied Optics **23(24)**, pp. 4486-4493, 1984